Journal of Biomechanics 45 (2012) 2577–2588

Contents lists available at SciVerse ScienceDirect

Journal of Biomechanics

journal homepage: www.elsevier.com/locate/jbiomech
www.JBiomech.com

Effects of pressure on arterial failure

Pannathai Khamdaengyodtai [a,b], Kambiz Vafai [b,*], Phrut Sakulchangsatjatai [a], Pradit Terdtoon [a]

[a] Department of Mechanical Engineering, Faculty of Engineering, Chiang Mai University, 50200, Thailand
[b] Department of Mechanical Engineering, University of California, Bourns Hall, Riverside, CA 92521-0425, United States

ARTICLE INFO

Article history:
Accepted 31 July 2012

Keywords:
Artery
Five layers
Three dimensional
Fiber reinforced material
Stress
Strain
Failure
Rupture

ABSTRACT

A three-dimensional multilayer model of mechanical response for analyzing the effect of pressure on arterial failure is presented in this work. The multilayer arterial wall is considered to be composed of five different layers. The three-dimensional effects are incorporated within the five-concentric axisymmetric layers while incorporating the nonlinear elastic characteristics under combined extension and inflation. Constitutive equations for fiber-reinforced material are employed for three of the major layers, i.e., intima, media and adventitia and an isotropic material model is employed for the other two layers, i.e., endothelium and internal elastic lamina. Our own developed three-dimensional five-layer model has been utilized to model propagated rupture area of the arterial wall. Required parameters for each layer are obtained by using a nonlinear least square method fitted to in vivo non-invasive experimental data of human artery and the effects of pressure on arterial failure are examined. The solutions from our computational model are compared with previous studies and good agreements are observed. Local stresses and strain distributions across the deformed arterial wall are illustrated and consequently the rupture area is predicted by varying luminal pressure in the physiological range and beyond. The effects of pressure on the arterial failure have been interpreted based on this comprehensive three-dimensional five-layer arterial wall model. This is the first study which employs two constitutive equations and incorporates a five-layer arterial wall model in three-dimensions based on in vivo non-invasive experimental data for a human artery.

1. Introduction

A cardiovascular system encompasses a pump (heart), a delivery network (arteries) and a return network (veins) to return the blood back to the pump to complete the cycle. The pressure resulting from the blood flow acts on the endothelium cells of an artery. The endothelium cells respond to stress and strain by inflation or contraction and extension. In this work, we analyze conditions under which arterial failure could occur. As such, the initiation and propagation of rupture area is predicted and an assessment of rupture area is qualitatively established. Mechanical properties of stress and strain of the arterial wall have received more attention in recent years. Several constitutive models have been proposed (Holzapfel et al., 2000; Delfino et al., 1997; Fung, 1990, 1997, 1993). Monolayer homogenous arterial wall is the simplest model to represent an artery. However, it is well known that the arterial wall is a non-homogeneous material. A better approach is to model heterogeneity of the arterial wall by considering it as a multi-layer structure while incorporating its architecture and its different layers, namely endothelium, intima, internal elastic lamina, media and adventitia. The pressure acting on the inside surface of arterial wall is caused by the lumen. While there are several definitions of stress and strain (Fung, 1969, 1994, 2001), in the present study, the Cauchy stress and the Green–Lagrange strain are used to refer to the force acting on the deformed area and the ratio of inflation and extension.

A biological tissue can be subjected to chemical changes, which can be effectively represented by changes in the stress and strain. By monitoring stress and strain during a cyclic load experiment, the response of an artery can be assessed during the loading and unloading processes (Holzapfel et al., 2004b). As such, stress and strain behavior of an arterial wall incorporating elastic deformation under a pressure load is investigated in this work. A three-dimensional five-layer model is established for studying the effect of pressure on the arterial failure. In particular, various pressure levels are studied and the rupture area is consequently predicted.

2. Analysis

2.1. Structure of an arterial wall

Typical histological and anatomical structure of an arterial wall is shown in Ai and Vafai (2006). The arterial wall is composed

* Corresponding author. Tel.: +1 951-827-2135; fax: +1 951-827-2899.
E-mail address: vafai@engr.ucr.edu (K. Vafai).

0021-9290/$ - see front matter © 2012 Elsevier Ltd. All rights reserved.
http://dx.doi.org/10.1016/j.jbiomech.2012.07.032

Nomenclature

$\boldsymbol{A}$	structure tensor of fiber direction
$\boldsymbol{a}$	acceleration vector
$\boldsymbol{a_o}$	fiber direction vector
$\boldsymbol{b}$	the left Cauchy Green tensor
$\boldsymbol{C}$	the right Cauchy Green tensor
c	stress-like parameter of isotropic term
DBP	diastolic blood pressure
$\boldsymbol{E}$	the Green-Lagrange strain tensor
$\boldsymbol{F}$	the deformation gradient tensor
$\boldsymbol{f}$	the body force tensor of blood
$\boldsymbol{G}$	the body force tensor of arterial wall
H	thickness of arterial layer
$\boldsymbol{I}$	identity tensor
I	principal invariant
k_1	stress-like parameter of anisotropic term
k_2	dimensionless parameter of anisotropic term
L	overall longitudinal length in reference configuration
MBP	mean blood pressure
MSE	mean square error
N	number of experimental data points
P	Lagrange multiplier
p	luminal pressure
R	radial position in reference configuration
r	radial position in deformed configuration
r_p	the Pearson product moment correlation coefficient
$\boldsymbol{S}$	the second Piola–Kirchhoff stress tensor
SBP	systolic blood pressure
T	period of cardiac time
t	time
U_o	reference bulk inflow velocity
u	velocity component
$\boldsymbol{v}$	velocity vector
$\boldsymbol{X}$	the position vector in reference configuration
$\boldsymbol{x}$	the position vector in deformed configuration
Z	longitudinal position in reference configuration
z	longitudinal position in deformed configuration

Greek symbols

β	angle of collagen fibers
δ	parameter for fluctuation of pulsatile flow
ζ	fold value of mean
Θ	angular position in reference configuration
θ	angular position in deformed configuration
λ	stretch ratio
μ	dynamic viscosity of blood
ξ	fold value of amplitude
ρ	density of arterial wall
$\boldsymbol{\sigma}$	the Cauchy stress tensor
Φ	opening angle
ψ	the strain energy function
Ω	the deformed configuration
Ω_o	the reference configuration

Superscript

$-$	deviator component
$*$	normalized value

Subscript

adv	adventitia
end	endothelium
i	inside
iel	internal elastic lamina
int	intima
j	arterial layer
med	media
o	outside
v	equivalent
vol	volumetric component
z	longitudinal direction

Other symbol

A_O	the average height above the abscissa
A_J	the height of the oscillation in terms of cosine
B_J	the height of the oscillation in terms of sine
$\boldsymbol{\nabla}$	gradient operator

of five layers. From the lumen side outward, the five layers of arterial wall are: endothelium, intima, internal elastic lamina (IEL), media and adventitia. The innermost layer, endothelium, is a single layer of endothelial cells lining the interior surface of the artery which are in direct contact with the lumen and could be elongated in the same direction as the blood flow (Yang and Vafai, 2006). Intima, the innermost major layer, consists of both connective tissue and smooth muscle. Intima grows with age or disease and consequently might become more significant in predicting the mechanical behavior of an arterial wall. The internal elastic lamina separates the intima from the media. The media, the thickest layer, consists of alternating layers of smooth muscle cells and elastic connective tissue which gives the media high strength and ability to resist the load. The media layer is surrounded by loose connective tissue, the adventitia. The adventitia is the outermost layer of the arterial wall, which is composed of fibrous tissue containing elastic fibers, lymphatic and occasional nutrient vessels. At high pressure levels, the adventitia behaves like a stiff tube to prevent the artery from rupture.

2.2. Stress and strain characteristics

Lets consider the body of an arterial wall in the reference configuration Ω_o. A material particle point in the cylindrical coordinate system is represented as $\boldsymbol{X}(R, \Theta, Z)$. After the arterial wall is deformed, the material point $\boldsymbol{X}(R, \Theta, Z)$ transforms to a new position designated as $\boldsymbol{x}(r, \theta, z)$. The transformation can be described by

$$\boldsymbol{F} = \frac{\partial \boldsymbol{x}}{\partial \boldsymbol{X}} \tag{1}$$

The deformation gradients can be used to describe the distance between two neighboring points in these two configurations and the Green–Lagrange strain tensor $\boldsymbol{E}$ can be introduced as

$$\boldsymbol{E} = \frac{1}{2}(\boldsymbol{C} - \boldsymbol{I}) \tag{2}$$

where the Green–Lagrange strain tensor $\boldsymbol{E}$ is given in terms of the right Cauchy Green tensor $\boldsymbol{C}$, which is

$$\boldsymbol{C}=\boldsymbol{F}^T\boldsymbol{F} \tag{3}$$

where $\boldsymbol{I}$ denotes the identity tensor.

The internal force within the deformed body per unit area can be represented as stress. To describe the hyperelastic stress response of an arterial wall, appropriate strain energy function ψ is chosen to describe its physical behavior. The force in the reference configuration Ω_o to its area, known as the second Piola–Kirchhoff stress tensor $\boldsymbol{S}$, could be determined by forming the first derivative of strain energy function ψ with respect to the Green–Lagrange strain tensor $\boldsymbol{E}$ as

$$\boldsymbol{S}=\frac{\partial\psi}{\partial\boldsymbol{E}} \tag{4}$$

The Piola–Kirchhoff stress tensor can be transformed onto the Cauchy stress tensor via the following relationship

$$\boldsymbol{\sigma}=J^{-1}\boldsymbol{F}\boldsymbol{S}\boldsymbol{F}^T \tag{5}$$

where J denotes the Jacobian determinant of the deformation gradient tensor which must satisfy the conservation of mass.

The Cauchy stress tensor $\boldsymbol{\sigma}$ could be expressed as the sum of two other stress tensors: volumetric stress tensor $\boldsymbol{\sigma}_{vol}$ which tends to change the volume of the stressed body and the stress deviator tensor $\overline{\boldsymbol{\sigma}}$ which tends to distort the stressed body, i.e.,

$$\boldsymbol{\sigma}=\boldsymbol{\sigma}_{vol}+\overline{\boldsymbol{\sigma}} \tag{6}$$

The equation of motion of a continuum derived by applying Newton's law can be expressed as

$$\frac{\partial\boldsymbol{\sigma}}{\partial\boldsymbol{x}}+\boldsymbol{G}=\rho\boldsymbol{a} \tag{7}$$

where $\boldsymbol{G}$ denotes the body force within the arterial wall and $\boldsymbol{a}$ denotes its acceleration.

The conservation of mass is expressed by

$$\frac{\partial\rho}{\partial t}+\frac{\partial\rho\boldsymbol{v}}{\partial\boldsymbol{x}}=\boldsymbol{0} \tag{8}$$

Where ρ denotes density of the arterial wall and $\boldsymbol{v}$ denotes its velocity vector.

The deformation of the arterial wall is related to the luminal pressure which in turn is due to the applied load by blood flow within the arterial lumen. The blood which can be represented as Newtonian fluid is described by the Navier–Stokes equation

$$\rho\frac{\partial v}{\partial t}+\rho\boldsymbol{v}\nabla\boldsymbol{v}=-\nabla p+\mu\nabla^2\boldsymbol{v}+\boldsymbol{f} \tag{9}$$

where ρ denotes the density of blood, $\boldsymbol{v}$, the velocity vector, p, the luminal pressure, μ, dynamic viscosity of blood and $\boldsymbol{f}$ denotes the body force. Hence, the stress and strain distributions in an arterial wall can be computed and used for predicting an arterial rupture.

2.3. Computational model

The schematic illustration of the arterial geometry and boundary conditions under consideration is shown in Fig. 1a. The arterial geometry is represented by five concentric axisymmetric nonlinear elastic layers. The luminal radius, R was taken as 3.1 mm along with the longitudinal length L of 124 mm (Yang and Vafai, 2006). The thickness of each arterial wall layer is presented in Fig. 1a (Yang and Vafai, 2006, 2008; Ai and Vafai, 2006). It is assumed that the pressure is uniform in the circumferential direction. The pressure on the outer arterial wall is assumed to be uniform with magnitude of 4 kPa. The five layers of the arterial wall are sequential, i.e., the outside radius of an individual wall layer is the same as the inside radius of its outward neighboring layer.

2.4. Mathematical formulation

There are six regions in the present mechanical model, i.e. lumen and five arterial layers of endothelium, intima, internal elastic lamina, media and adventitia. In what follows, the mathematical formulation for each layer is presented.

2.4.1. Lumen

The pressure profile from experimental data ($N=5852$) for a human carotid artery obtained by UEIL [Ultrasound and Elasticity Imaging Laboratory (UEIL) at the Biomedical Engineering and Radiology department of Columbia University, NY, US] is shown in Fig. 1b. Blood flow is pulsatile and characterized by a parabolic velocity profile at the inlet of the arterial lumen. Considering an axisymmetric flow and neglecting the gravitational effect, the Navier–Stokes equations can be presented as

$$\frac{\partial p}{\partial r}=0,\ \frac{\partial p}{\partial\theta}=0,\ \rho\frac{\partial u_z}{\partial t}+u_z\frac{\partial u_z}{\partial z}=-\frac{\partial p}{\partial z}+\mu\frac{\partial^2 u_z}{\partial r^2}+\mu\frac{\partial^2 u_z}{\partial z^2} \tag{10}$$

The time dependent outlet pressure, $p_{outlet}(t)$ along a cardiac cycle could be obtained by curve fitting utilizing a Fourier approximation with mean squares error fit of a sinusoidal function (Chapra and Canale, 2010) with the experimental data for the pressure. So, the pressure within a cardiac cycle and its variation along the longitudinal direction, $p(z,t)$, can be expressed as

$$p(z,t)=\left(\frac{2\mu U_o}{R^2}\left(1+\delta sin\left(\frac{2\pi t}{T}\right)\right)\right)(z_{outlet}-z)+\varsigma A_o+\xi\sum_{J=1}^{30}A_J cos\left(J\frac{2\pi t}{T}\right)+B_J sin\left(J\frac{2\pi t}{T}\right) \tag{11}$$

where $\mu=0.0037\ g/mm\ s$, U_o is the reference bulk inflow velocity, $U_o=169\ mm/s$, δ is the pulsatile flow parameter, $\delta=1$, T is cardiac period, $T=0.8$ s, parameters ζ and ξ are equal to unity, parameter A_O is 12011 Pa and A_J and B_J are given in Table 1.

2.4.2. Arterial layers

The geometry and boundary conditions are shown in Fig. 1a. Kinematics of the artery in cylindrical coordinate system can be described as (Ai and Vafai, 2006; Yang and Vafai, 2008)

$$r=\sqrt{\frac{R^2-R_i^2}{k\lambda_z}+r_i^2}, \tag{12}$$

$$\theta=k\Theta+Z\frac{\Phi}{L}, \tag{13}$$

$$z=\lambda_z Z \tag{14}$$

where $k=2\pi/2\pi-\alpha$, λ_z is the stretch ratio in longitudinal direction (Delfino et al., 1997), Φ and L are the opening angle and overall length of artery in the reference configuration and subscript i in Eq. (12) refers to the inner part of the artery. An artery deformed under extension and inflation and without residual strain is considered in this study.

For endothelium and internal elastic lamina, the strain energy function of neo-Hookean has been used to determine the nonlinear response. The strain energy function for an incompressible neo-Hookean material is

$$\overline{\psi}_j=\frac{c_j}{2}(\bar{I}_1-3) \tag{15}$$

where $c_j>0$ is the stress-like parameter, $\bar{I}_1$ is the first principal invariant of $\overline{\boldsymbol{C}}$ and subscript j refers to the endothelium and internal elastic lamina (IEL). For intima, media and adventitia, utilizing an artery structure composted of fibers and non-collagen matrix of material and fiber reinforced strain energy function suggested by Holzapfel et al. (2000) is suitable to relate stress and

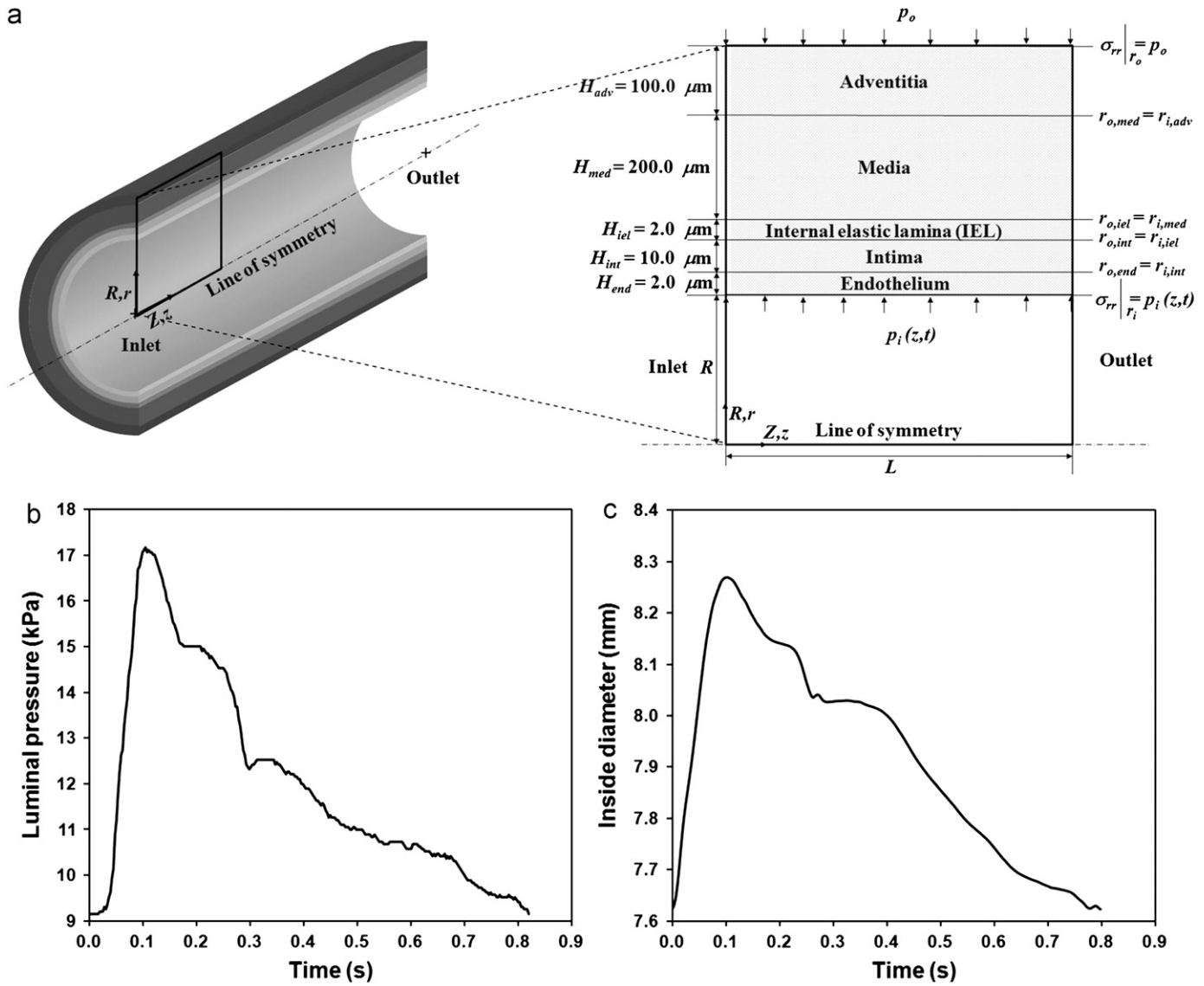

Fig. 1. (a) Schematic illustration of an artery and the imposed boundary conditions, (b) the pressure profile along a cardiac cycle for a human carotid artery (male, time step=0.140014 ms, N=5852 points, cardiac cycle time=time step*(N−1)=0.8192 s, heart rate=73.240 bpm, Khamdaeng et al., 2012a) and (c) the diameter profile along a cardiac cycle for a human carotid artery (time step=1/505 ms, N=404 points, cardiac cycle time=time step*(N−1)=0.7980 s, heart rate=75.186 bpm, Khamdaeng et al., 2012b).

Table 1
Parameters A_J and B_J in units of Pascal.

A_J						B_J					
A_1	−307.802	A_{11}	−8.0677	A_{21}	−14.8198	B_1	2472.354	B_{11}	6.7722	B_{21}	−0.7861
A_2	−1152.17	A_{12}	44.5415	A_{22}	−35.7354	B_2	899.1454	B_{12}	−21.8575	B_{22}	4.3848
A_3	−904.308	A_{13}	22.2471	A_{23}	−5.9142	B_3	141.6018	B_{13}	40.6469	B_{23}	−19.529
A_4	−472.175	A_{14}	−30.1193	A_{24}	4.3074	B_4	−162.328	B_{14}	−5.9916	B_{24}	−17.2017
A_5	−376.189	A_{15}	18.2471	A_{25}	−1.4468	B_5	−319.284	B_{15}	−3.3656	B_{25}	−20.3007
A_6	−12.2606	A_{16}	21.6265	A_{26}	22.4666	B_6	−490.187	B_{16}	33.2005	B_{26}	−15.6279
A_7	196.7156	A_{17}	9.0006	A_{27}	14.0872	B_7	−193.917	B_{17}	11.1883	B_{27}	6.0502
A_8	93.4258	A_{18}	7.895	A_{28}	8.5244	B_8	−52.9216	B_{18}	21.7935	B_{28}	−2.0939
A_9	76.1842	A_{19}	−14.0034	A_{29}	8.0986	B_9	−44.6953	B_{19}	37.0081	B_{29}	−0.6531
A_{10}	70.6487	A_{20}	−20.9844	A_{30}	6.8244	B_{10}	58.292	B_{20}	7.7842	B_{30}	9.3357

strain. This fiber reinforced strain energy function takes into account the architecture of the arterial wall and also requires a relatively small number of parameters (Khakpour and Vafai, 2008; Holzapfel et al., 2004b, 2005b). The strain energy function which will incorporate the isotropic and anisotropic parts can be written as

$$\overline{\psi}_j = \frac{c_j}{2}(\bar{I}_1 - 3) + \frac{k_{1j}}{2k_{2j}} \sum_{i=4,6} \{exp[k_{2j}(\bar{I}_{ij} - 1)] - 1\} \quad (16)$$

where $c_j > 0$, $k_{1j} > 0$ are stress-like parameters and $k_{2j} > 0$ is a dimensionless parameter, subscript j refers to intima, media and adventitia layers and subscript i refers to the index number of invariants. In Eq. (16), $\overline{I}_1$ is the first principal invariant of $\overline{\boldsymbol{C}}$. The definitions of the invariants associated with the anisotropic deformation of arterial wall are given below

$$\overline{I}_{4j} = \overline{\boldsymbol{C}} : \boldsymbol{A}_{1j},\ \overline{I}_{6j} = \overline{\boldsymbol{C}} : \boldsymbol{A}_{2j} \tag{17}$$

The collagen fibers normally do not support a compressive stress. Thus, in case of $\overline{I}_4 \le 1$ and $\overline{I}_6 \le 1$ the response is similar to the response of a rubber like material as described by Neo-Hookean functions. The tensor $\boldsymbol{A}_{1j}$ and $\boldsymbol{A}_{2j}$ characterizing the structure are given by

$$\boldsymbol{A}_{1j} = \boldsymbol{a}_{o1j} \otimes \boldsymbol{a}_{o1j}, \boldsymbol{A}_{2j} = \boldsymbol{a}_{o2j} \otimes \boldsymbol{a}_{o2j} \tag{18}$$

Components of the direction vector $\boldsymbol{a}_{o1j}$ and $\boldsymbol{a}_{o2j}$ in cylindrical coordinate system are

$$\boldsymbol{a}_{o1j} = \begin{bmatrix} 0 \\ cos\beta_j \\ sin\beta_j \end{bmatrix},\ \boldsymbol{a}_{o2j} = \begin{bmatrix} 0 \\ cos\beta_j \\ -sin\beta_j \end{bmatrix} \tag{19}$$

where β_j is the angle between the collagen fibers and circumferential direction. Three different values of 5^o, 7^o and 49^o (Holzapfel et al., 2002) are applied for the three major layers of intima, media and adventitia, respectively.

Hence, the stress in Eulerian description could be determined by the expression given below.

$$\overline{\sigma}_j = c_j dev\overline{\boldsymbol{b}} + \sum_{i=4,6} 2\overline{\psi}_{ij} dev(\boldsymbol{a}_{ij} \otimes \boldsymbol{a}_{ij}) \tag{20}$$

where $dev\overline{\boldsymbol{b}} = \overline{\boldsymbol{b}} - 1/3[\overline{\boldsymbol{b}} : \boldsymbol{I}]\boldsymbol{I}$, $dev(\boldsymbol{a}_{ij} \otimes \boldsymbol{a}_{ij}) = (\boldsymbol{a}_{ij} \otimes \boldsymbol{a}_{ij}) - 1/3[(\boldsymbol{a}_{ij} \otimes \boldsymbol{a}_{ij}) : \boldsymbol{I}]\boldsymbol{I}$, $\boldsymbol{a}_{ij} = \overline{\boldsymbol{F}}\boldsymbol{a}_{oij}$ denotes the Eulerian counter part of $\boldsymbol{a}_{oij}$ and $\overline{\psi}_{ij} = \partial\overline{\psi}_{aniso}/\partial\overline{I}_{ij}$ denotes a response function i.e. $\overline{\psi}_{4j} = k_1(\overline{I}_{4j} - 1)(exp(k_2(\overline{I}_{4j} - 1)^2))$ and $\overline{\psi}_{6j} = k_1(\overline{I}_{6j} - 1)(exp(k_2(\overline{I}_{6j} - 1)^2))$. Additionally, it should be noted that $\boldsymbol{F} = (J^{1/3}\boldsymbol{I})\overline{\boldsymbol{F}}$, $\overline{\boldsymbol{C}} = \overline{\boldsymbol{F}}^T\boldsymbol{F}$ and $\overline{\boldsymbol{b}} = \overline{\boldsymbol{F}}\overline{\boldsymbol{F}}^T$. When incompressibility of an arterial wall is considered we obtain, $\boldsymbol{F} = \overline{\boldsymbol{F}}$, $\boldsymbol{C} = \overline{\boldsymbol{C}}$ and $\boldsymbol{b} = \overline{\boldsymbol{b}}$. There are only three parameters to be considered for each layer c, k_1 and k_2.

2.5. Determination of constitutive parameters

The diameter profile from experimental data (N=404) at carotid artery of human supported by UEIL (Ultrasound and Elasticity Imaging Laboratory (UEIL), Biomedical Engineering and Radiology, Columbia University, NY, US) are shown in Fig. 1c. To obtain the diameter the ultrasound probe is placed on the skin at the carotid position. The minima and maxima of the pressure and diameter waveforms are aligned and matched over the cardiac cycle. The viscosity effect is hence ignored. Arterial wall is considered as an incompressible material and horizontal so the gravity effect could be ignored, thus

$$\frac{\partial\boldsymbol{\sigma}}{\partial\boldsymbol{x}} = \boldsymbol{0} \tag{21}$$

Luminal pressure could be determined by

$$p_i = \int_{r_i}^{r_o} (\overline{\sigma}_{\theta\theta} - \overline{\sigma}_{rr})\frac{dr}{r} + p_o \tag{22}$$

where $\sigma_{\theta\theta} = P + \overline{\sigma}_{\theta\theta}$, $\sigma_{rr} = P + \overline{\sigma}_{rr}$ and P is the Lagrange multiplier used to enforce the incompressibility constraint.

Moving boundary has to be incorporated when analyzing the five-layer model. The moving boundary is normalized. Numerical integration with a three-point Gaussian quadrature which has an accuracy of the order of five is employed to discretize Eq. (22). Nonlinear least square method is used to estimate the relevant parameters by minimizing the mean square error MSE_{par} of luminal pressures (Objective function) given by

$$MSE_{par} = \frac{1}{N}\sum_{i=1}^{N}\left(p_{i,model} - p_{i,experiment}\right)^2 \tag{23}$$

The Pearson product moment correlation coefficient r_p through the data points in $p_{i,model}$ and $p_{i,experiment}$ is used to assess the strength of the fit. The equation for the Pearson product moment correlation coefficient is

$$r_p = \frac{\sum_{i=1}^{N}\left(p_{i,model} - \overline{p}_{i,model}\right)\left(p_{i,experiment} - \overline{p}_{i,experiment}\right)}{\sqrt{\sum_{i=1}^{N}\left(p_{i,model} - \overline{p}_{i,model}\right)^2 \sum_{i=1}^{N}\left(p_{i,experiment} - \overline{p}_{i,experiment}\right)^2}} \tag{24}$$

where N is the number of data points and i is the index for the summation over the whole data points.

2.6. Arterial rupture

If the pressure is high and the artery has an inappropriate deformation, the rupture of the arterial wall could occur. There are a number of researchers who have studied the ultimate tensile stress and associated stretch in a normal human artery (Holzapfel, 2001; Zohdi et al., 2004; Franceschini et al., 2006; Sommer et al., 2008; Mohan and Melvin, 1982, 1983). In the past decade ultimate values of separated layers has been studied (Sommer et al., 2008; Holzapfel et al., 2005a,b, 2004a; Holzapfel, 2009; Zhao et al., 2008; Sommer, 2010). The ultimate tensile stress and associated ultimate stretch (Holzapfel et al., 2004b) shown in Table 2 in circumferential and longitudinal directions for intima, media and adventitia are used as criteria for assessing the rupture of the arterial wall in the present study.

The equivalent tensile stress σ_v and strain E_v could be computed from the Cauchy stress tensor and the Green–Lagrange strain tensor as

$$\sigma_v = \sqrt{\frac{3}{2}\left(\boldsymbol{\sigma} : \boldsymbol{\sigma} - \frac{(tr\boldsymbol{\sigma})^2}{3}\right)} \tag{25}$$

$$E_v = \sqrt{\frac{3}{2}\left(\boldsymbol{E} : \boldsymbol{E} - \frac{(tr\boldsymbol{E})^2}{3}\right)} \tag{26}$$

The ultimate tensile stress and the associated ultimate stretch in Table 2 are determined for critical equivalent tensile stress $\sigma_{vj,cri}$ and strain $E_{vj,cri}$. Two strategies are investigated to identify the rupture area of the arterial wall. The first strategy is based on strain values. The area of arterial wall where the local equivalent strain exceeds the critical values is defined to be a rupture area. The second strategy is based on the tensile stress. The area of the

Table 2
The ultimate tensile stress and associated ultimate stretch for intima, media, and adventitia

Layer	Direction	Ultimate tensile stress (kPa)	Ultimate stretch
Adventitia	Circumferential direction	1031.6	1.44
	Longitudinal direction	951.8	1.353
Media	Circumferential direction	202	1.27
	Longitudinal direction	188.8	1.536
Intima	Circumferential direction	488.6	1.331
	Longitudinal direction	943.7	1.255

arterial wall where the local equivalent tensile stress and the associated local equivalent strain exceed the critical values is defined to be the rupture area. Estimation of the rupture risk is referred to as the local equivalent of stress and strain approach. The percentage of the rupture risk of the arterial wall P_{risk} is defined as

$$P_{risk} = 100\sigma_j^* E_j^* \tag{27}$$

where σ_j^* and E_j^* are normalized values which can be presented as

$$\sigma_j^* \left\{ \sigma_j^* \middle| if \frac{\sigma_v}{\sigma_{vj,cri}} < 1, \sigma_j^* = \frac{\sigma_v}{\sigma_{vj,cri}}; if \frac{\sigma_v}{\sigma_{vj,cri}} \geq 1, \sigma_j^* = 1 \right\}, \tag{28}$$

$$E_j^* \left\{ E_j^* \middle| if \frac{E_v}{E_{vj,cri}} < 1, E_j^* = \frac{E_v}{E_{vj,cri}}; if \frac{E_v}{E_{vj,cri}} \geq 1, E_j^* = 1 \right\} \tag{29}$$

Due to lack of data for endothelium and internal elastic lamina (IEL) layers, critical values for intima are applied for these two layers.

3. Results and discussion

3.1. Comparison with previous studies

This is the first study which employs two constitutive equations and incorporates a five-layer arterial wall model in three-dimensions based on in vivo non-invasive experimental data for a human artery. Our computational model is compared to a number of prior studies for one and two-layer material models by using their constitutive equations and material parameter sets in our in-house computational program. We have compared our comprehensive model with the pertinent results in the literature in Figs. 2 and 3. This constitutes a detailed set of nine comparisons which are highlighted in Table 3. The source of comparison, constitutive equations and utilized parameters for these comparisons are given in Table 3.

Fig. 2 displays four comparisons for the one-layer model computed by our computational program representing the luminal pressure versus inner and outer radii with prior works

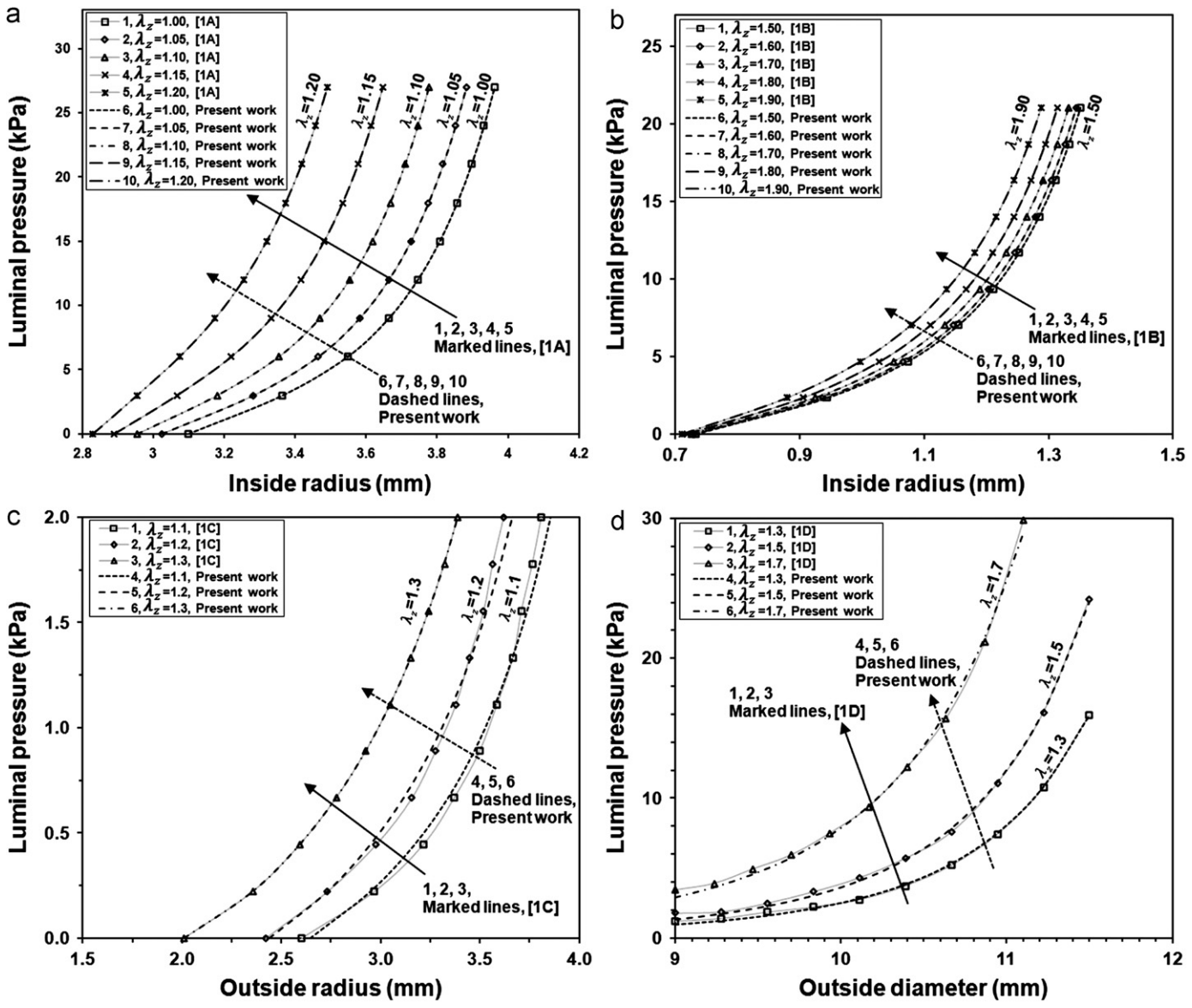

Fig. 2. Comparison of luminal pressure versus inside and outside radii for a one layer artery with prior works listed in Table 3 (a) Case 1A, (b) Case 1B, (c) Case 1C and (d) Case 1D.

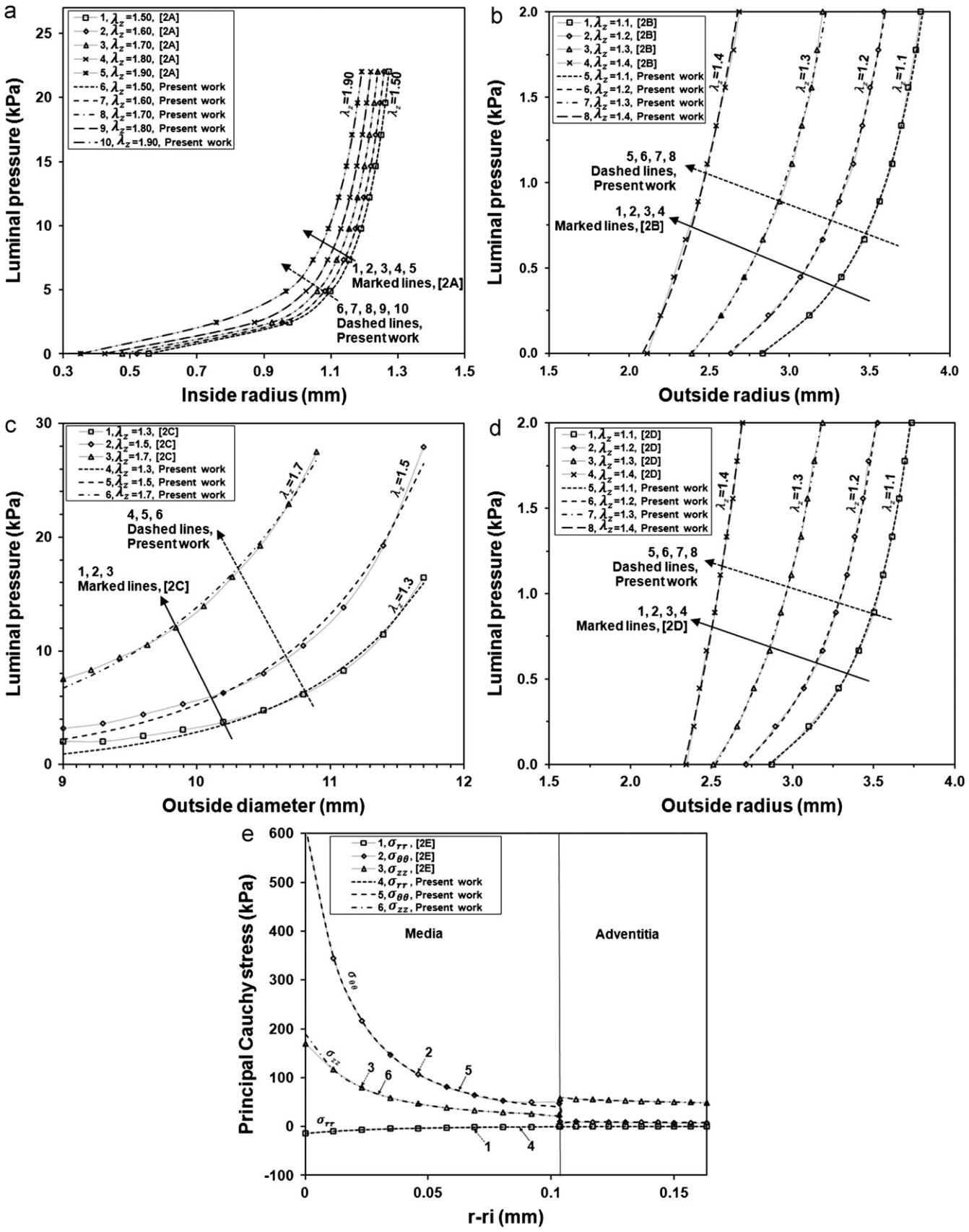

Fig. 3. Comparison of luminal pressure versus inside and outside radii and the principal Cauchy stresses across arterial wall for a two-layer artery with prior works listed in Table 3 (a) Case 2A, (b) Case 2B, (c) Case 2C, (d) Case 2D and (e) Case 2E.

Table 3
List of comparisons with our computational model, specifying the number of layers, source of comparison and the constitutive equation

Fig.	Case	Number of layers	Source of comparison	Constitutive equation	Utilized parameters
2a	1A	1	Holzapfel et al. (2000)	Delfino et al. (1997)	Artery; $a=44.2$ kPa and $b=16.7$
2b	1B	1	Holzapfel et al. (2000)	Fung's type	Artery; $c=26.95$ kPa and $b_1=0.9925$ $b_2=0.4180$, $b_3=0.0089$, $b_4=0.0749$, $b_5=0.029$, $b_6=0.0193$ and $b_7=5.000$
2c	1C	1	Sokolis (2010)	Fung's type	Esophagus; $c=2.0934$ kPa, $b_1=0.783$, $b_2=7.385$, $b_4=0.611$
2d	1D	1	von Maltzahn et al. (1984)	Fung's type	Artery; $c=2.4657$*2 kPa, $b_1=0.1499$, $b_2=1.6409$ and $b_4=0.0028/2$
3a	2A	2	Holzapfel et al. (2000)	Holzapfel et al. (2000)	Media; $c=3.000$ kPa, $k_1=2.3632$ kPa and $k_2=0.8393$ Adventitia; $c=0.3000$ kPa, $k_1=0.5620$ kPa and $k_2=0.7112$
3b	2B	2	Sokolis (2010)	Fung's type	Mucosa–submucosa; $c=1974.4$ Pa, $b_1=3.296$, $b_2=11.529$ and $b_4=1.847$ Muscle; $c=1012.6$ Pa, $b_1=0.568$, $b_2=5.197$ and $b_4=0.360$
3c	2C	2	von Maltzahn et al. (1984)	Fung's type	Media; $c=2.4657$*2 kPa, $b_1=0.1499$, $b_2=1.6409$ and $b_4=0.0028/2$ Adventitia; $c=9.1140$*2 kPa, $b_1=0.1939$, $b_2=1.2601$ and $b_4=0.7759/2$
3d	2D	2	Sokolis (2010)	Fung's type	Mucosa–submucosa; $c=2406.1$ Pa, $b_1=2.220$, $b_2=10.229$ and $b_4=1.747$ Muscle; $c=1012.6$ Pa, $b_1=0.568$, $b_2=5.197$ and $b_4=0.360$
3e	2E	2	Holzapfel et al. (2000)	Holzapfel et al. (2000)	Media; $c=3.000$ kPa, $k_1=2.3632$ kPa and $k_2=0.8393$ Adventitia; $c=0.3000$ kPa, $k_1=0.5620$ kPa and $k_2=0.7112$

Note: Strain energy function of Delfino et al. (1997), $\overline{\psi}=a/b\{exp(b/2(\bar{I}_1-3))-1\}$, Strain energy function of Fung's type, $\overline{\psi}=1/2c[exp(\overline{Q})-1]$, $\overline{Q}=b_1\overline{E}^2_{\Theta\Theta}+b_2\overline{E}^2_{ZZ}+b_3\overline{E}^2_{RR}+2b_4\overline{E}_{\Theta\Theta}\overline{E}_{ZZ}+2b_5\overline{E}_{ZZ}\overline{E}_{RR}+2b_6\overline{E}_{RR}\overline{E}_{\Theta\Theta}+b_7\overline{E}^2_{\Theta Z}+b_8\overline{E}^2_{RZ}+b_9\overline{E}^2_{R\Theta}$, Strain energy function of Holzapfel et al. (2000), $\overline{\psi}=1/2c(\bar{I}_1-3)+k_1/2k_2\sum_{i=4,6}\left\{exp[k_2(\bar{I}_i-1)^2]-1\right\}$.

Table 4
Estimated stress related parameters for different arterial layers.

Layer	Optimized parameters		
	c [kPa]	k_1 [kPa]	k_2
Endothelium	250.9108	–	–
Intima	270.9837	2.1492	1.3012
IEL	250.9108	–	–
Media	100.3643	3.5820	5.2049
Adventitia	10.0364	0.0716	0.9759

(Cases 1A, 1B, 1C and 1D shown in Table 3). Our simulations are found to be in very good agreement with previous studies. Slight differences in the results occur due to different solution methodologies.

Fig. 3 displays five comparisons for the two-layer model computed by our computational model representing luminal pressure versus inner and outer radii (Cases 2A, 2B, 2C and 2D) and the principal Cauchy stresses across arterial wall (Case 2E). Again, very good agreement with prior works is observed. The computational program is extended to calculate the stress and strain distributions across inflated and extended arterial wall incorporating the five-layer three-dimensional model. The obtained results are analyzed to investigate circumstances under which the arterial wall will rupture.

3.2. Parameter estimation

The estimated parameters are shown in Table 4 and the Pearson product moment correlation coefficient r_p of 0.97 is obtained. Using these estimated parameter sets, the strain energy density contours in circumferential and longitudinal directions are investigated for each of the arterial layers.

3.3. Effects of pressure on arterial rupture

The pressure load acting on the inner surface of the arterial wall increases the associated strain continually to the point of failure. Deformation of the arterial wall could be presented directly by displaying the strain distribution. As such the strain distribution can be used to identify the rupture area. This is done in Fig. 4. The rupture area can be identified using both the stress and strain distributions such as the results presented in Fig. 5.

From the result shown in Fig. 5 the rupture characteristics can be qualitatively interpreted. The failure process can be separated into two regimes, failure initiation and failure propagation. The existence and extent of the failure initiation and propagation depends on the pressure or stress which relates to the arterial geometry or strain by the properties of each arterial layer. It could be seen that the rupture occurs in the circumferential direction around the arterial wall and the rupture initiates a tear at the medial surface of the artery. Moreover, the rupture propagates from inside the medial surface towards the outer surface.

In order to quantitatively interpret the effect of pressure on arterial failure, an assessment is made regarding the percentage for the risk of rupture. The percentage for the risk of rupture is displayed in Fig. 6. The risk level is divided into five groups. First, the normal pressure level is when the pressure is lower than 16.0 kPa. In the normal pressure level range it is found that maximum percentage risk of rupture does not exceed 50% (Fig. 6a). The second level, pre-high pressure level is when the pressure is in the range of 16.0–18.7 kPa. At pre-high pressure level, maximum risk percentage of rupture is much greater but does not exceed 80% (Fig. 6b). Next, high pressure level is when the pressure is in the range of 18.7–21.3 kPa. At this level, maximum risk percentage of rupture is quite high but rupture is not eminent (Fig. 6c). The rupture initiation and propagation occurs within the severe pressure level which is between 21.3 and 26.7 kPa (Fig. 6d and e). The rupture initiation occurs at about 24.0 kPa.

This study has explored a comprehensive model based on in vivo non-invasive experimental data to identify rupture area and estimate the risk percentage of rupture in normal five-layer arterial wall. The major advantages of the present model is that it incorporates the architecture of arterial layers by using two suitable forms of constitutive equations to describe the mechanical attributes. In addition, the luminal pressure variations resulting from the luminal blood flow is included in this study.

4. Conclusions

The effects of pressure on arterial failure have been investigated based on a comprehensive three-dimensional five-layer arterial wall model. The endothelium and internal elastic lamina are treated as isotropic media and intima, media and adventitia

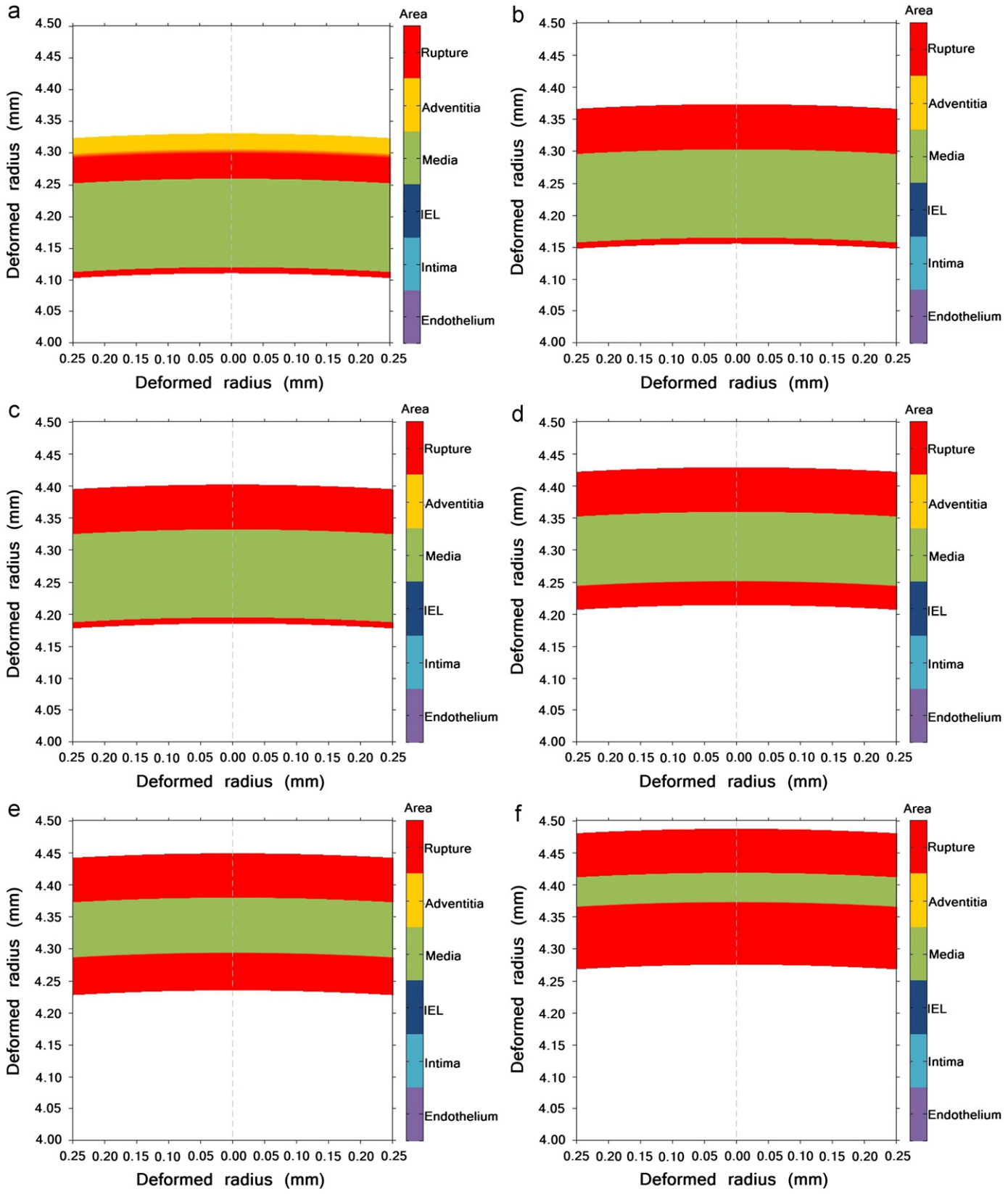

Fig. 4. Rupture characteristics of an arterial wall based on utilizing strain as a criterion. (a)–(f) illustrates the wall deformation in the $r-\theta$ plane at luminal pressure of 16.0, 18.7, 21.3, 24.0, 26.7 and 33.3 kPa, respectively. There are five colors to identify different layers, i.e. violet for endothelium, light blue for intima, dark blue for internal elastic lamina (IEL), green for media and yellow for adventitia. Rupture area is identified with a red color.

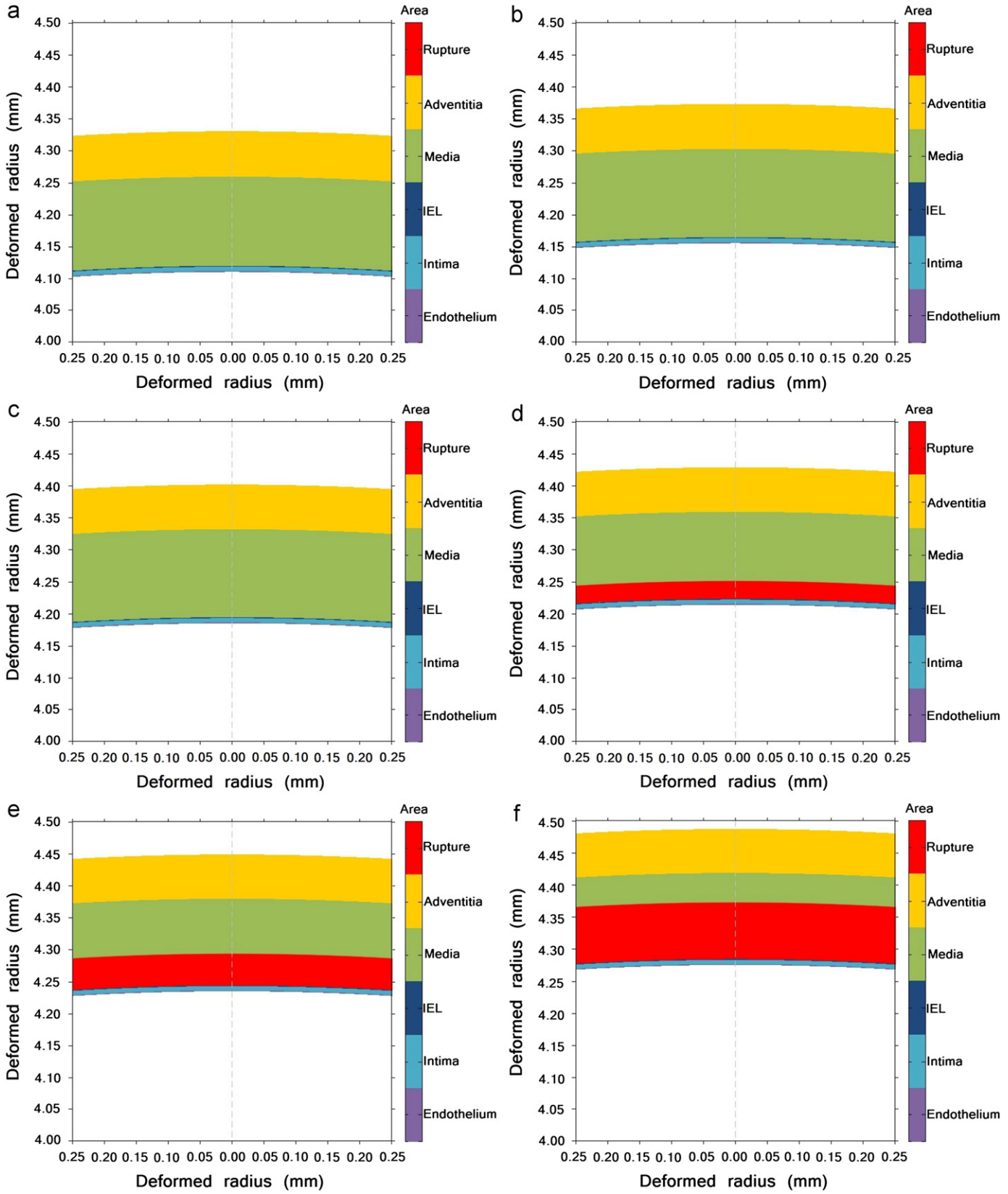

Fig. 5. Rupture characteristics of an arterial wall based on using stress and strain as a criterion. (a)–(f) illustrates the wall deformation in the $r-\theta$ plane at luminal pressure of 16.0, 18.7, 21.3, 24.0, 26.7 and 33.3 kPa, respectively. There are five colors to identify different layers, i.e. violet for endothelium, light blue for intima, dark blue for internal elastic lamina (IEL), green for media and yellow for adventitia. Rupture area is identified with a red color.

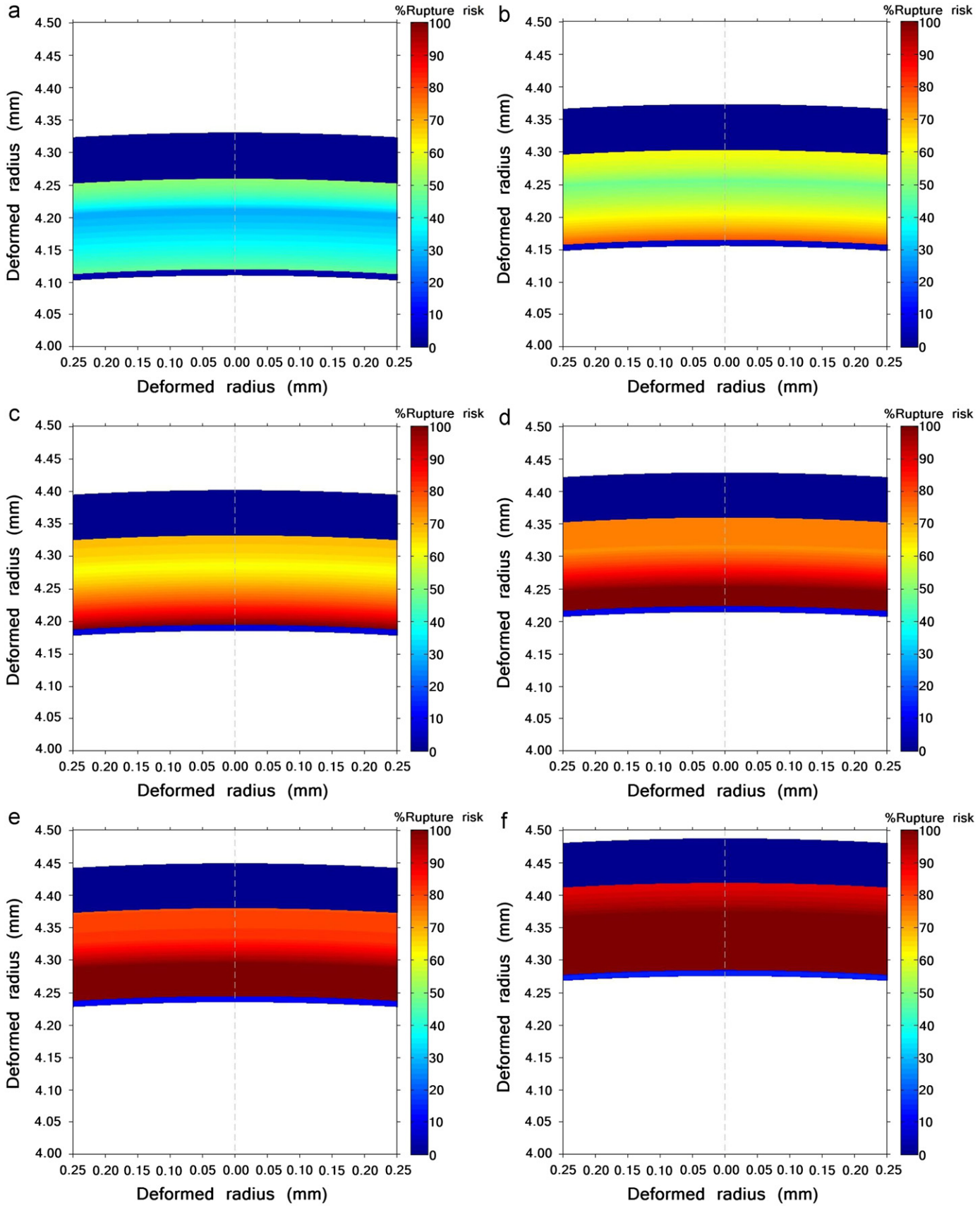

Fig. 6. Percentage risk of rupture of an arterial wall based on using stress and strain as a criterion, (a)–(f) illustrates the risk percentage of rupture in the $r-\theta$ plane at luminal pressures of 16.0, 18.7, 21.3, 24.0, 26.7 and 33.3 kPa, respectively.

are treated as anisotropic media incorporating the active collagen fibers. Layered arterial wall is modeled using two types of constitutive equations. Our comprehensive model was found to be in very good agreement with the results from the prior studies. The effects of pressure on arterial failure are examined in detail. The present investigation demonstrates that the pressure is mainly responsible for the concentric wall movement. The present work incorporates the three-dimensional five-layer model and predicts the propagated rupture area of the arterial wall coupled with blood flow in the lumen.

Conflict of interest statement

There is no conflict of interest for this paper.

Acknowledgments

Financial support from the Thailand Research Fund through the Royal Golden Jubilee Ph.D. Program (PHD/0181/2549) to P. Khamdaengyodtai and P. Terdtoon is acknowledged. The authors are also grateful to Associate Professor Elisa E. Konofagou of Ultrasound and Elasticity Imaging Laboratory, Biomedical Engineering and Radiology, Columbia University, NY, for the useful data and Kazue Okajima, M.D., Ph.D., from Columbia University Medical Center, for acquiring the tonometry data.

References

Ai, L., Vafai, K., 2006. A coupling model for macromolecule transport in a stenosed arterial wall. International Journal of Heat and Mass Transfer 49, 1568–1591.

Chapra, S.C., Canale, R.P., 2010. Numerical Methods for Engineers. McGraw-Hill Higher Education, p. 968.

Delfino, A., Stergiopulos, N., Moore, J.E., Meister, J.J., 1997. Residual strain effects on the stress field in a thick wall finite element model of the human carotid bifurcation. Journal of Biomechanics 30, 777–786.

Franceschini, G., Bigoni, D., Regitnig, P., Holzapfel, G.A., 2006. Brain tissue deforms similarly to filled elastomer and follows consolidation theory. Journal of the Mechanics and Physics of Solid 54, 2592–2620.

Fung, Y.C., 1969. A First Course in Continuum Mechanics. Prentice-Hall 301p.

Fung, Y.C., 1990. Biomechanics: Motion, Flow, Stress and Growth. Springer-Verlag 569p.

Fung, Y.C., 1993. Biomechanics: Mechanical properties of living tissues. Springer-Verlag 568p.

Fung, Y.C., 1994. A First Course in Continuum Mechanics: For Physical and Biological Engineers and Scientists. Prentice-Hall 311p.

Fung, Y.C., 1997. Biomechanics: Circulation. Springer 571p.

Fung, Y.C., 2001. Classical and Computational Solid Mechanics. World Scientific 930p.

Holzapfel, G.A., 2001. Biomechanics of Soft Tissue, Lemaitre Handbook of Material Behavior Models. Academic Press 1057–1071.

Holzapfel, G.A., 2009. Arterial Tissue in Health and Disease: Experimental Data, Collagen-Based Modeling and Simulation, Including Aortic Dissection, Biomechanical Modeling at the Molecular, Cellular and Tissue Levels. Springer 259–343.

Holzapfel, G.A., Gasser, T.C., Ogden, R.W., 2000. A new constitutive framework for arterial wall mechanics and a comparative study of material models. Journal of Elasticity 61, 1–48.

Holzapfel, G.A., Gasser, T.C., Ogden, R.W., 2004a. Comparison of a multi-layer Structural model for arterial walls with a Fung-type model, and issues of material stability. Transactions of the ASME 126, 264–275.

Holzapfel, G.A., Gasser, T.C., Ogden, R.W., 2005a. Comparison of a structural model with a Fung-type model using a carotid artery: Issues of material stability. In: Proceedings of the 1st GAMM Seminar on Continuum Biomechanics No. II-14. 79–89.

Holzapfel, G.A., Sommer, G., Gasser, C.T., Regitnig, P., 2005b. Determination of layer-specific mechanical properties of human coronary arteries with nonatherosclerotic intimal thickening and related constitutive modeling. American Journal of Physiology Heart Circulation Physiology 289, H2048–H2058.

Holzapfel, G.A., Sommer, G., Regitnig, P., 2004b. Anisotropic mechanical properties of tissue components in human atherosclerotic plaques. Journal of Biomechanical Engineering 126, 657–665.

Holzapfel, G.A., Stadler, M., Schulze-Bauer, C.A.J., 2002. A layer-specific three-dimensional model for the simulation of balloon angioplasty using magnetic resonance imaging and mechanical testing. Annals of Biomedical Engineering 30, 753–767.

Khakpour, M., Vafai, K., 2008. Critical assessment of arterial transport models, Int. Journal Heat and Mass Transfer 51, 807–822.

Khamdaeng, T, Terdtoon, P., Sakulchangsatjatai, P., Kammuang-lue, N., 2012a. The human aortic stiffness determination using the carotid stiffness and pulse wave velocity relation in vivo. Journal of Science and Technology Mahasarakham University 5, 31.

Khamdaeng, T., Luo, J., Vappou, J., Terdtoon, P., Konofagou, E.E., 2012b. Arterial stiffness identification of the human carotid artery using the stress-strain relationship in vivo. Ultrasonics 52, 402–411.

Mohan, D., Melvin, J.W., 1982. Failure properties of passive human aortic tissue. I-uniaxial tension tests. Journal of Biomechanics 15 (11), 887–902.

Mohan, D., Melvin, J.W., 1983. Failure properties of passive human aortic tissue. II-biaxial tension tests. Journal of Biomechanics 16 (1), 31–44.

Sokolis, D.P., 2010. Strain-energy function and three-dimensional stress distribution in esophageal biomechanics. Journal of Biomechanics 43, 2753–2764.

Sommer, G., 2008. Mechanical properties of healthy and diseased human arteries, Monographic Series TU Graz. Computer Engineering and Science 7, 19–67.

Sommer, G., Gasser, T.C., Regitnig, P., Auer, M., Holzapfel, G.A., 2008. Dissection properties of the human aortic media: An experimental study. Journal of Biomechanical Engineering 130 (2) 021007-1-12.

von Maltzahn, W.W., Warriyar, R.G., Keitzer, W.F., 1984. Experimental measurements of elastic properties of media and adventitia of bovine carotid arteries. Journal of Biomechanics 17 (11), 839–847.

Yang, N., Vafai, K., 2006. Modeling of low-density lipoprotein (LDL) transport in the artery-effects of hypertension. International Journal of Heat and Mass Transfer 49, 850–867.

Yang, N., Vafai, K., 2008. Low-density lipoprotein (LDL) transport in an artery—a simplified analytical solution. International Journal Heat and Mass Transfer 51, 497–505.

Zhao, A., Field, M.L., Digges, K., Richens, D., 2008. Blunt trauma and acute aortic syndrome: a three layer finite-element model of the aortic wall. European Journal of Cardio-thoracic Surgery 34, 623–629.

Zohdi, T.I., Holzapfel, G.A., Berger, S.A., 2004. A phenomenological model for atherosclerotic plaque growth and rupture. Journal of Theoretical Biology 227, 437–443.